A Superhydrophobic TiO2-Polymer Nanocomposite Surface with UV-Induced Reversible Wettability and Self-Cleaning Properties.

5 AUTHORS, INCLUDING:

Yang Liu
City University of New York - College of Staten …
5 PUBLICATIONS **41** CITATIONS

Bikash Mondal
City University of New York - College of Staten …
7 PUBLICATIONS **80** CITATIONS

Alan Lyons
City University of New York - College of Staten …
51 PUBLICATIONS **453** CITATIONS

Superhydrophobic TiO₂−Polymer Nanocomposite Surface with UV-Induced Reversible Wettability and Self-Cleaning Properties

Qian Feng Xu, Yang Liu, Fang-Ju Lin, Bikash Mondal, and Alan M. Lyons*

Department of Chemistry, College of Staten Island, City University of New York, New York, New York 10314, United States

Ⓢ *Supporting Information*
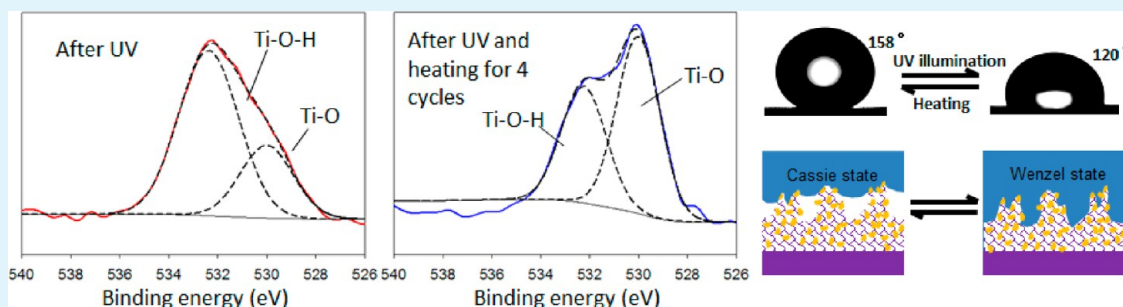
ABSTRACT: Multifunctional superhydrophobic nanocomposite surfaces based on photocatalytic materials, such as fluorosilane modified TiO₂, have generated significant research interest. However, there are two challenges to forming such multifunctional surfaces with stable superhydrophobic properties: the photocatalytic oxidation of the hydrophobic functional groups, which leads to the permanent loss of superhydrophobicity, as well as the photoinduced reversible hydrolysis of the catalytic particle surface. Herein, we report a simple and inexpensive template lamination method to fabricate multifunctional TiO₂−high-density polyethylene (HDPE) nanocomposite surfaces exhibiting superhydrophobicity, UV-induced reversible wettability, and self-cleaning properties. The laminated surface possesses a hierarchical roughness spanning the micro- to nanoscale range. This was achieved by using a wire mesh template to emboss the HDPE surface creating an array of polymeric posts while partially embedding untreated TiO₂ nanoparticles selectively into the top surface of these features. The surface exhibits excellent superhydrophobic properties immediately after lamination without any chemical surface modification to the TiO₂ nanoparticles. Exposure to UV light causes the surface to become hydrophilic. This change in wettability can be reversed by heating the surface to restore superhydrophobicity. The effect of TiO₂ nanoparticle surface coverage and chemical composition on the mechanism and magnitude of wettability changes was studied by EDX and XPS. In addition, the ability of the surface to shed impacting water droplets as well as the ability of such droplets to clean away particulate contaminants was demonstrated.

KEYWORDS: *superhydrophobic/philic surfaces, titanium dioxide, composite materials, hierarchical structures, functional coatings*

1. INTRODUCTION

Superhydrophobic surfaces with a water contact angle (CA) larger than 150° and a slip angle (SA) less than 10°[1−6] have attracted significant attention because of their unique water repellency, which may lead to applications ranging from micro/nanofluidic devices to large area self-cleaning building products.[7−13] Recently, efforts have been made to fabricate multifunctional superhydrophobic surfaces based on semiconductor oxide materials such as TiO₂, ZnO, and V₂O₅.[14−36] Such semiconductor materials are widely used in photocatalysis, solar energy conversion and various sensors.[16,37−41] In addition, TiO₂ surfaces have been shown to exhibit antimicrobial properties, useful for hospital[39] and food processing[40] applications, because of its photocatalytic properties. Exposing semiconductor particles to UV radiation has enabled the fabrication of surfaces which exhibit light-induced switching of the wetting properties of droplets between superhydrophobic and hydrophilic states. Storage in the dark for extended periods of time or heating restores the superhydrophobic proper-

ties.[17,27] Reversible wetting increases the functionality of these surfaces and can increase their usefulness for microfluidic devices.[18]

In general, to achieve superhydrophobicity, low surface energies and high surface roughness values are required. Because most semiconductor oxides are relatively hydrophilic materials under visible light,[41] their surfaces must either be modified chemically, to lower the surface energy, or synthesized with a specific morphology to generate a hierarchal roughness in order to achieve superhydrophobicity. For V₂O₅[26] and ZnO,[27−33] chemical surface modification is not required to achieve superhydrophobicity; extreme surface roughness is sufficient. The fabrication of a superhydrophobic TiO₂ surface, based on morphological roughness alone, has proven to be more challenging. In part, this is due to the greater

hydrophilicity of the surface as well as its greater photo-reactivity. For example, many rough TiO_2 surfaces have been made to exhibit superhydrophobic properties by treating the surface with a fluorosilane, fatty acid or other hydrophobic reagents.[18−23,25,42−50] Also, TiO_2 has been codeposited with hydrophobic polymers such as polytetrafluoroethylene[35] and polydimethylsiloxane[36] to achieve superhydrophobicity and catalytic activity. However, the valuable properties afforded by the semiconductor, such as photocatalyzed surface reactions, would be reduced or even eliminated by chemical surface modification.[51] In addition, exposure to broadband UV light for certain time will result in the photocatalytic decomposition of these surface layers, irreversibly rendering the surface hydrophilic.

In two cases, superhydrophobic TiO_2 surfaces exhibiting reversible wetting were fabricated without resorting to chemical surface modification.[17,52] In these reports, the TiO_2 surfaces exhibited a hierarchical roughness over a significant range of length scales. This was achieved through the growth of particles with extreme topography. However, the slip angles are either relatively high $(13°)$,[52] or not reported.[17] This relatively high roll-off angle indicates a significant interaction between water and the untreated TiO_2 surface, limiting the applicability of such superhydrophobic surfaces. Thus, it remains a challenge to concurrently achieve high CA, low SA, and high photocatalytic activity directly from pure TiO_2 materials without surface modification.

Although several superhydrophobic TiO_2 surfaces with reversible wetting characteristics have been demonstrated (with or without surfactants), the surfaces may not be viable for device fabrication for two reasons: cost of fabrication and reliability. The growth conditions used to synthesize the requisite topography required for reversible TiO_2 surfaces are harsh and require long reaction times. Such processes would be expensive and difficult to scale. The use of commercially available TiO_2 particles would reduce costs and broaden the range of potential applications.

In this paper, we present a simple and inexpensive lamination templating process for fabricating a superhydrophobic TiO_2−polymer nanocomposite surface that exhibits UV-induced reversible wettability. By creating a surface with multiple roughness length scales, ranging from tens of micrometers to tens of nanometers, superhydrophobic properties are achieved without the use of chemical surface modification (e.g., slianes). Thus the TiO_2 surface is exposed and in direct contact with the fluid. Primary roughness is produced by laminating a wire mesh template against a high density polyethylene (HDPE) film. Pores in the mesh create isolated, elevated regions (or posts) on the polymer surfaces that are impregnated with TiO_2 nanoparticles. The use of preformed, commercially available TiO_2 nanoparticles and conventional polymer processing equipment enable the use of low-cost fabrication processes that are compatible with large scale manufacturing. The effect of UV illumination on CA was studied as a function of exposure time, the presence of water and the extent of surface coverage of TiO_2 nanoparticles. Heat was used to reverse the UV induced wetting and restore the superhydrophobic properties. The reversibility was demonstrated over 4 cycles and the mechanism was characterized by XPS. Self-cleaning properties of the surface were also experimentally demonstrated.

2. EXPERIMENTAL SECTION

Materials, Methods, and Surface Fabrication. A commercially available thermoplastic sheet of HDPE from McMaster-Carr was used as the polymer substrate. A precision woven nylon mesh (371 × 371, from McMaster-Carr) was used as a template to create microstructures on the polymer surface. The wire diameter and the pore size of the nylon mesh are 33 and 36 μm, respectively. Two kinds of nanoparticles were used to create nanostructures on the polymer surface. One was TiO_2 nanoparticles (634662, from Sigma-Aldrich) with a size ranging from 20 to 100 nm (TEM images in Figure 1).
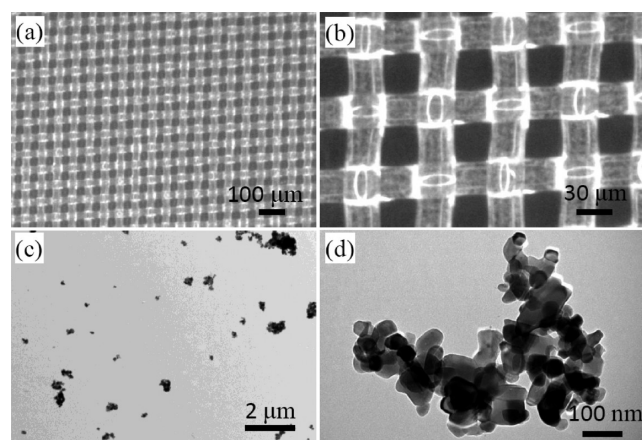

Figure 1. (a, b) Optical images of nylon mesh template, and (c, d) TEM images of TiO_2 particles. Panels b and d are higher-magnification views of panels a and c, respectively.

According to the producer, the phase of the TiO_2 particles was a mixture of 31% rutile and 69% anatase.[53] The other type of particle is fumed SiO_2 (TS530, from Cabot Corp.) with an average size of 150 nm. The procedure for fabricating surfaces involves two processing steps as shown schematically in Figure 2. A similar process was discussed previously for the fabrication of superhydrophobic surfaces from polymers without nanoparticles.[54] In the first step, a piece of HDPE sheet, a mesh template and a layer of nanoparticles are laminated together under heat and pressure with the targeted polymer surface facing the mesh template and the nanoparticles. The layer of nanoparticles was coated using a Doctor Blade method. The stack-up was heated to 138 °C under a pressure of 4000 psi for 30 min and then cooled to room temperature. In the second step, the mesh template and excess nanoparticles are separated from the polymer film. The fabricated superhydrophobic surface is formed and exposed during the peeling process. The surface was cleaned using ultrasonic bath before use.

Droplet Impingement and Self-Cleaning Test. The fabricated superhydrophobic surfaces were mounted on a translation stage driven by a motor at a speed of 1 mm s^{-1}. The tilt angle of the surface was fixed at a certain angle. Water droplets were pumped out by a syringe pump (KD Scientific) at a speed of 1 μL s^{-1} for the droplet impingement test, and at a speed of 8 μL s^{-1} for the self-cleaning test. The distance between the surface and tip was adjusted over a range from 5 to 100 mm. Both coarse Al_2O_3 sand with a size ranging from 50 to 130 μm and fine carbon powders with an average size of 1 μm were used as test contaminates. The impingement and the self-cleaning process were recorded by a high speed camera (EX-FH25, Casio) at 240 and 120 frames per second, respectively.

UV Illumination Experiments. The UV light was generated by a UV spot lamp (Bluewave 200, from Dymax) using a 5 mm diameter liquid light guide. The power density was set at 33 mW cm^{-2}. The wavelength of the UV light ranged from 320 to 450 nm. The UV illumination was conducted with and without water on the superhydrophobic surface at room temperature (∼25 °C). The change of the CA under the UV illumination was monitored at specific time intervals. The surface illuminated under water was dried by
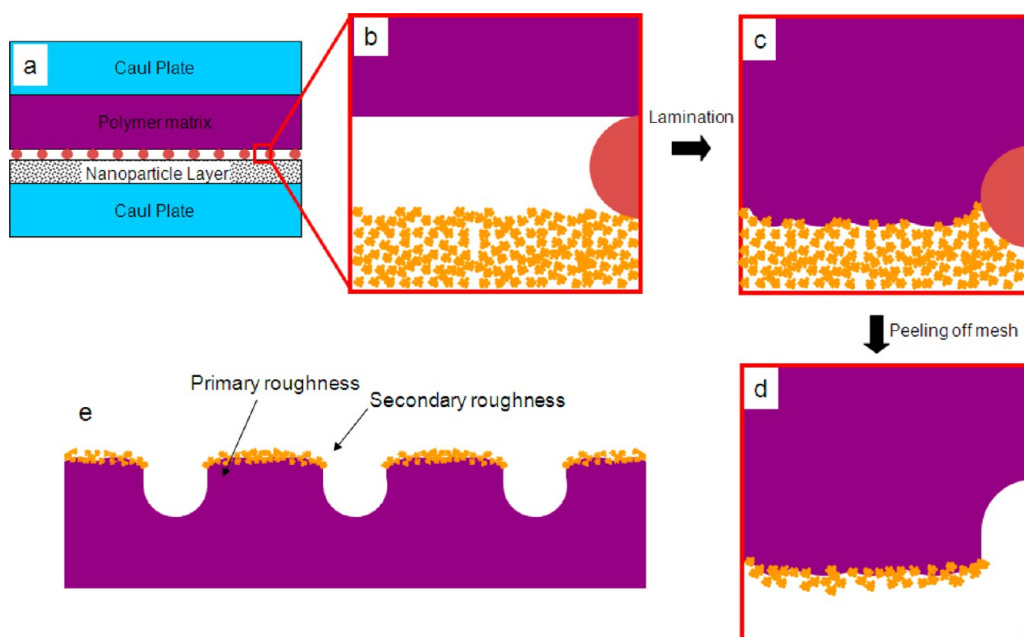
Figure 2. Schematic of the formation of the microstructures during the processing.

compressed air before the CA measurements. For thermal recovery of superhydrophobic properties, the surface was heated in a dark oven at 105 °C for 1.5 h after UV illumination. No attempt was made to determine the minimum heating time required to achieve recovery of superhydrophobic properties and times less than 1.5 h may be sufficient.

Characterization. The thermal properties of the HDPE were measured by differential scanning calorimetry (DSC) using a TA Instruments model Q100 at a heating rate of 10 °C min^{-1}. Surface structures were studied by field emission scanning electron microscopy (FESEM, Amary) and optical microscopy (Nikon-SMZ 1500 and Laborlux-12ME). The static CAs and slip angle were measured with a goniometer (250-F1, rame-hart Instrument Co). Droplets of distilled water, with a volume of 5 μL were placed gently onto the surface at room temperature and pressure. The static CA and advancing and receding CAs were measured five times at different locations such that the measurement variance was ±2°. The slip angle was measured by placing water droplets of ∼10 μL on an initially horizontally substrate and then tilting the substrate until the water droplet rolled off. SA was also measured by placing droplets on a surface tilted to a specific angle and determining the angle below which droplets would adhere to the surface. The chemical composition of the surfaces was studied by X-ray photoelectron spectroscopy (XPS) using an Omicron Nanotechnology system (EA-125) with monochromatic radiation from an Al target. The XPS examination was carried out immediately after the surface fabrication as well as after UV irradiation and heat treatment. The distribution of TiO$_2$ particles on the fabricated surfaces were detected by energy-dispersive X-ray spectroscopy (EDX) at a scanning voltage of 10 KV.

3. RESULTS AND DISCUSSION

3.1. Fabrication of TiO$_2$–Polymer Nanocomposite Surface.
HDPE was selected as the polymer substrate as it is inexpensive, environmentally friendly (e.g., recyclable and nontoxic), and mechanically tough and can be stabilized against aging through the incorporation of antioxidants. In addition, HDPE possesses a low surface energy and exhibits a contact angle of ∼105° with water. Smooth HDPE sheets are usually easy to clean, but they cannot be self-cleaning, because small water droplets adhere firmly to the surface and cannot roll-off. For achieving a low slip angle (SA), a superhydrophobic surface

is required. To achieve superhydrophobicity, a micro and/or nanoscale rough surface structure is necessary because it can dramatically reduce the liquid–solid contact area, and thus the adhesion forces between water and the solid surface. Super-hydrophobic properties can be further improved by creating hierarchical levels of roughness[55,56] such that the primary, relatively large scale, roughness keeps the droplet elevated above the surface for stability and reduces the overall liquid–solid contact area while the fine scale roughness (i.e., secondary roughness) minimizes solid–liquid contact in the area of the primary roughness. The combined primary and secondary roughness length scales forms a hierarchical roughness that is essential for fabricating a robust superhydrophobic surface, especially when the fine scale roughness is formed from nanoparticles composed of hydrophilic materials (i.e., materials with water contact angles <90°).

To create a surface with multiple roughness scales, we used a lamination templating method, similar to one described previously,[57] but modified to include TiO$_2$ nanoparticles. A precision polymer nylon woven mesh with a wire diameter of 33 μm and a square pore size of 36 μm was used to create primary roughness microstructures (Figure 1a,b), and TiO$_2$ nanoparticles (Figure 1c,d) were used to create the fine scale roughness nanostructures. As shown in images c and d in Figure 1 the TiO$_2$ nanoparticles are composed of single TiO$_2$ particles with a size ranging from 15 to 100 nm. These individual particles are formed into larger agglomerates with a size of ∼500 nm. This agglomeration thus forms an additional roughness hierarchy.

The lamination procedure is simple. A lamination temperature of 138 °C was used to ensure that the HDPE was above the crystalline melt point of 132.6 °C (as determined by DSC and shown in the Supporting Information, Figure SF1). During lamination, the molten polymer flows into the open pores (36 × 36 μm) of the mesh and adheres to the TiO$_2$ agglomerates as shown schematically in Figure 2a–c. Flow is limited by the viscosity of the polymer (where the viscosity depends upon the temperature and molecular weight of the polymer) and applied
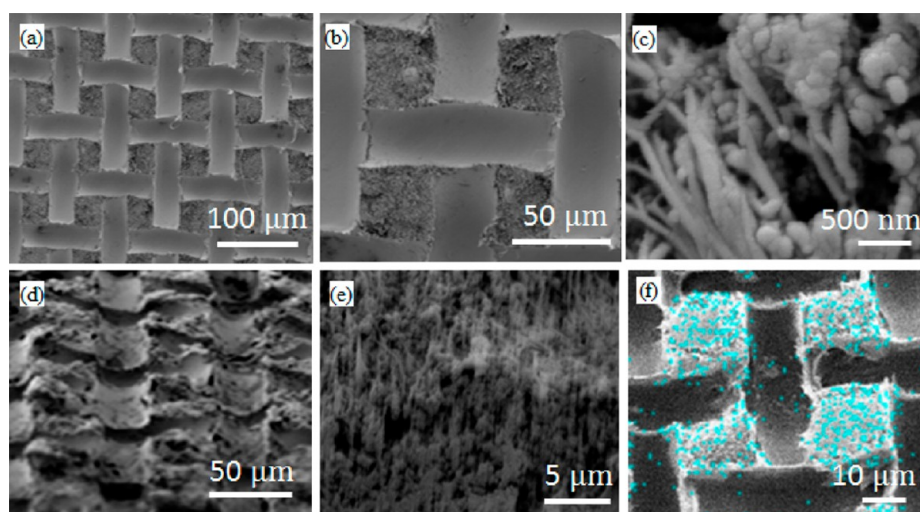
8917

dx.doi.org/10.1021/am401668y | ACS Appl. Mater. Interfaces 2013, 5, 8915−8924

Figure 3. (a−e) SEM images of the fabricated surfaces: (a−c) top view and (d, e) cross view tilted at 80° and 87° respectively. (f) EDX image, showing the nano TiO$_2$ distribution on the surface.

pressure. After lamination, the stack was cooled to room temperature (25 °C) and the mesh was separated from the polymer film by peeling. Because the nanoparticles prevent the molten polymer from flowing around the mesh wires, the mesh could be easily peeled off the HDPE surface. Excess TiO$_2$ nanoparticles were removed during the peeling step, however ultrasonicating the surface in distilled water ensured that all excess particles were removed (Figure 2d, e).

The structure of the fabricated surface was studied by SEM to gain insight into surface roughness hierarchy. Typical SEM images recorded at low and high magnifications and from different viewing angles are shown in Figure 3a−e. In images a and b in Figure 3, it can be seen that the fabricated surface is composed of microscale square posts (69 μm pitch) surrounded by curved grooves formed from the embossed wire mesh template. The side length of the square posts is about 36 μm, and the height of the posts varies with the curvature of the woven mesh (Figure 3d). Nanoscale features on the top surface of the posts can be clearly discerned under higher magnification (Figure 3c), and these nanostructures are composed of both TiO$_2$ nanoparticles and HDPE. The polymer forms a web-like structure with a filament diameter ranging from 80 to 500 nm, whereas the aggregates of TiO$_2$ nanoparticles are fully or partially embedded into the polymer surface. The size of the TiO$_2$ aggregates after lamination is consistent with the TEM images of the as-received nano-particles (Figure 1c, d). Figure 3e is taken from 87° angle under high magnification and shows that the filaments appear aligned with each other and perpendicular to the substrate surface.

To investigate the effect of concentration and distribution of the TiO$_2$ nanoparticles, we used energy-dispersive X-ray spectroscopy (EDX) for mapping the location of TiO$_2$ nanoparticles on the surface. The surface was coated with carbon to improve the conductivity for imaging. The high- and low-magnification EDX images are shown in Figure 3f and Figure SF2 in the Supporting Information, respectively. It can be seen that the TiO$_2$ nanoparticles are primarily located on the tops of the posts; only a very few TiO$_2$ particles can be detected on the grooves surrounding the posts. This distribution is consistent with the process described in the preceding paragraphs. Although the surface was precoated with carbon for imaging, the detected weight ratio of elemental Ti to C is about 37: 53, indicating a high concentration of TiO$_2$ nanoparticles on the posts.

3.2. Superhydrophobic Properties. TiO$_2$ is intrinsically hydrophilic[17] such that the contact angle of a water droplet on a smooth crystal of TiO$_2$ is 72−74°. Conversely, HDPE is intrinsically hydrophobic. Combining these two materials into a segregated hybrid surface with hierarchical roughness results in a superhydrophobic material; no chemical surface treatment is required. For comparison, the contact angle of a layer of TiO$_2$ nanoparticles deposited on a glass slide was measured. The deposit was formed by dip-coated the slide into a methanol solution containing 2.5% TiO$_2$ nanoparticles 5 times followed by drying in an oven. The TiO$_2$-glass surface showed superhydrophilicity; water spread rapidly across the surface. The measured CA of this surface was less than 10° as shown in Figure 4a. In contrast, the static water CA measured on the TiO$_2$−HDPE polymer nanocomposite surface was 158° using a water droplet of 5 μL as shown in Figure 4b. The water droplet appears like a transparent ball on the surface as shown in Figure 4c. Water droplets less than 4 μL could not to be placed onto the surface because the adhesion force between the micro syringe tip and the water droplet was greater than the total force from gravity and the adhesion force between the water droplet and the fabricated solid surface. The slip angle of 10 μL water droplets was measured to be ∼8° by using a tilting base method (base angle was increased from 0° at a rate of 5°/s). A much lower SA, <4°, was measured when placing water droplets on a pretilted surface.

The high static CA angle and low SA clearly show excellent superhydrophobic properties. To more fully understand the wetting behavior of the surface, the advancing and receding CA were also studied. As shown in images c and d in Figure 4, the advancing and receding CA was measured (using the method of increasing and decreasing the droplet volume) to be 159 and 152°, respectively. The contact angle hysteresis ($\theta_{adv} - \theta_{rec}$) is only 7°. According to previous studies, the SA angle is proportional to the CAH and can be calculated using the relationship developed by Furmidge[58] and modified by Extrand.[59] This can be written as

$$\sin \alpha = \frac{2w}{\pi mg}\gamma_{LV}(\cos \theta_R - \cos \theta_A) \tag{1}$$
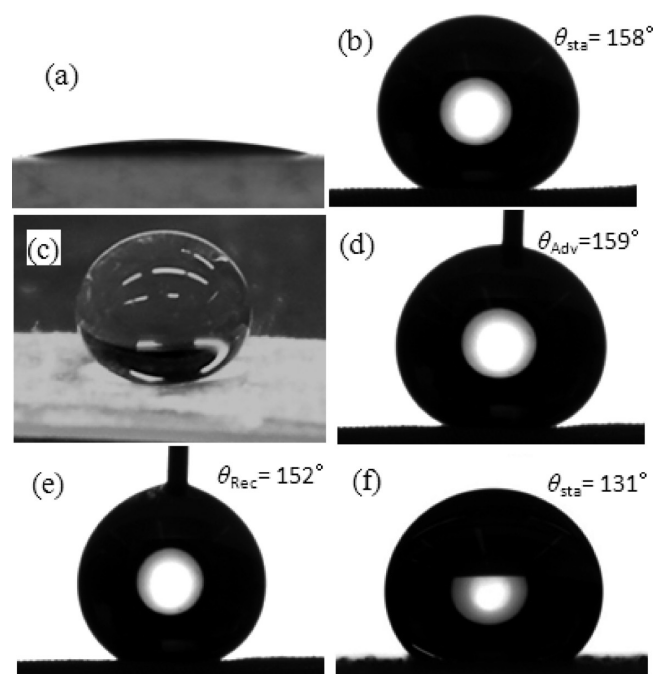
Figure 4. (a) Static CA on a surface made by dip-coating a glass slide with a methanol solution containing 0.25% nano TiO$_2$ particles, (b–e) static CA, optical picture of a water droplet, advancing CA, and receding CA on the fabricated TiO$_2$–HDPE nanocomposite surface, respectively. (f) Static CA on a surface made by spilling glass beads on a flat PDMS substrate.

where γ, m, w, and g are the liquid–vapor surface tension, mass of the droplet, width of the droplet, and the acceleration due to gravity respectively. θ_A/θ_R are the apparent advancing and receding contact angles, and α is the critical angle of inclination or slip angle. Using this equation, a slip angle (SA) of 6.4° would be predicted, in good agreement with the experimentally measured value for a pretilted surface. The low slip angle value measured confirms the correlation between a low slip angle and low CAH.

In the present case, the apparent contact area is composed of three kinds of interfaces: the water-TiO$_2$, water-HDPE and water–air interfaces. So, the Cassie[60−62] equation could be written as $\cos \theta_C = r_1 f_1 \cos \theta_1 + r_2 f_2 \cos \theta_2 + f_3 \cos \theta_3$, where the θ_C is the observed contact angle with water in the Cassie state, θ_1, θ_2 and θ_3 are the theoretical CAs of the three liquid interfaces (with TiO$_2$, HDPE and air), r_1, r_2 are the roughness coefficients (true area/projected area) for the TiO$_2$ and HDPE surfaces ($r_3 = 1$), and f_1, f_2, and f_3 are the projected wetted fractions of the three interfaces along the surface, with $f_1 + f_2 +$

$f_3 = 1$. Because of the high particle density, small gaps between TiO$_2$ particles and filamentary form of the HDPE on the top surface, most of the HDPE and some of the TiO$_2$ particles would not be wetted as shown schematically in Figure 5. Thus, f_2 would approach 0 (as only air contacts the HDPE).

The theoretical CA of TiO$_2$ (θ_1) could vary over a range from 0 to 74° depending on the exposed crystal plane and the number of water molecules and hydroxyl groups on the TiO$_2$ surface. For a freshly prepared sample, we can assume that θ_1 is approximately 70° because the TiO$_2$ nanoparticles were relatively dry and polycrystalline and stored in a sealed brown bottle before use. The CAs of θ_2 and θ_3 are 105 and 180°, respectively.

From observations of water on this surface, an air–water interface can be clearly observed in the grooved regions. From geometric calculations, the groove areas account for 73% of the total areal surface percentage. Wetting on the top surface of the posts could potentially occur on two materials: TiO$_2$ and HDPE. On the basis of the EDX study, the weight ratio of Ti:C is 37:53 on the top surface of the post which would correspond to a TiO$_2$: polyethylene weight ratio of approximately 1:1. The TiO$_2$: polymer volume ratio is estimated to be 1: 5 using 4.2 and 0.9 g/cm^3 for the density of the TiO$_2$ nanoparticles and HDPE, respectively. Assuming the water contacts all exposed TiO$_2$ surfaces and no HDPE surfaces, Then $f_1 = 0.05$ and $f_3 = 0.95$. This coverage estimate is approximate as it depends upon the distribution of TiO$_2$ particles through the thickness of the surface as well as the effect of the surface roughness on X-ray escape depth. If we assume that the TiO$_2$ particles are spherical with half their surface embedded in the HDPE, then $r_1 \approx 2$. Substituting values for θ, r_1, and f_1–f_3 into the modified Cassie equation, then θ_C was calculated to be 156°. This value of θ_C agrees well with the measured static CA of 158°.

After UV exposure, the entire surface becomes wetted. The contact angle of TiO$_2$ is assumed to be 10° and an approximation of 2 is used for the roughness of HDPE. In this case, θ_C was calculated to be 113°. This value of θ_C agrees reasonably well with the measured static CA of 120°.

A mixed hydrophilic–hydrophobic surface could retain air in the plastron more effectively compared to superhydrophobic surfaces made from only hydrophobic materials. To visually demonstrate this effect, a relatively large-scale composite model surface was constructed from 100 μm diameter glass beads coated onto a flat, hydrophobic PDMS substrate. A water droplet (~20 μL) placed on this surface showed a high CA of 131° as shown in Figure 4f. Many air bubbles were trapped between the glass beads and could be clearly observed under an optical stereo microscope due to the relatively large size of the glass beads and the gaps between them. Similarly, trapping of
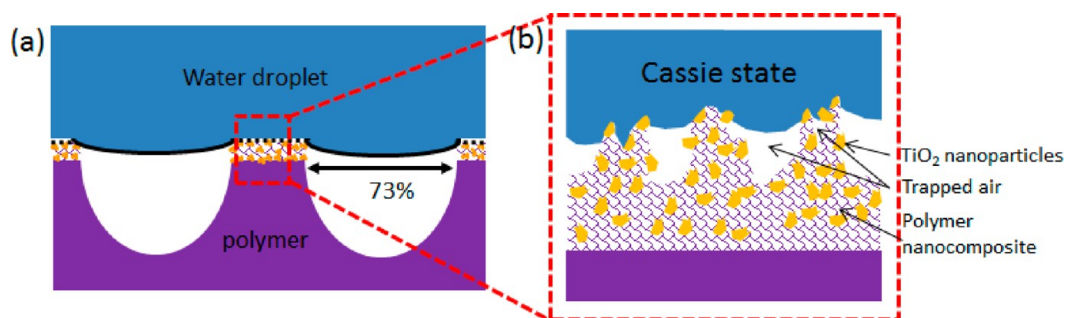

Figure 5. Schematics of water–air interface on the fabricated TiO$_2$–polymer nanocomposite surface with hierarchical structures.

air between surface features is expected to occur on the TiO$_2$–HDPE surface found on the top of the posts as shown schematically in Figure 5. This is consistent with the behavior of *Salvinia* leaves,[63] which are able to effectively retain air even under high water flow rates.

The stability of a droplet on the surface was studied in an environmental chamber for a period of 24 h. The Cassie state was found to be metastable, transitioning gradually to a Wenzel state over the course of one day. (Slip angle increased to 30° after 12 h and the droplet became pinned to the surface after 24 h). This metastability is not surprising as TiO$_2$ will slowly hydrolyze in water; UV light accelerates this rate as discussed in the paper. As shown in Figure 7, section 3.5, the transition to the Wenzel state occurs in less than 25 min when a surface is illuminated with UV light in the presence of water and 90 min when UV illumination is conducted in ambient relative humidity. When hydrophobic silica nanoparticles were used in place of TiO$_2$, the droplet remained in the Cassie state for >24 h with no change in contact angle or slip angle.

3.3. Mechanical Stability of the TiO$_2$–HDPE Nanocomposite.
To assess the stability of the TiO$_2$–HDPE superhydrophobic surfaces, we observed water droplets impinging onto the surfaces. The materials were mounted onto glass substrates using double-sided tape to create macroscopically flat surfaces. The glass substrate was then tilted at an angle of 4°. Water droplets (8 μL) were released from a height of 30 mm above the surface and the impingement was recorded with a high speed camera at a speed of 240 frames per second. A sequence of extracted images from one experiment (video SI1 in the Supporting Information) is shown in Figure SF3 in the Supporting Information. It can be seen that the water droplet recoils after impacting the surface, impacts a second time and rolls off the surface. More interestingly, from Figure SF3 in the Supporting Information, it can be seen that a smaller, satellite droplet (<1 μL) was ejected during the initial impingement of the primary droplet. This satellite droplet bounced again when it fell on the surface and bounced/rolled off the surface. The ability for such a small droplet to bounce off the surface indicates stable superhydrophobic properties as the Laplace pressure across such a droplet is quite high making it susceptible to rupture on a solid surface with coarse features.[64] The phenomena of water droplets bouncing and ejecting small, satellite droplets, has been attributed to the excess gas pressure generated by compressing air into the pores at the impinging moment[65] as well as a function of droplet velocity.[66,67]

For comparison, a superhydrophobic surface was made using the same method but with hydrophobic SiO$_2$ nanoparticles instead of TiO$_2$ nanoparticles. Water droplets again bounced up and easily rolled off this SiO$_2$–HDPE surface. However, no satellite droplets were observed, even though the volume and release height of the droplets were held constant. One explanation may be that the hydrophilic TiO$_2$ particles could more effectively pin the droplet than the hydrophobic SiO$_2$ particles. Thus the droplet would be elongated and tend to split during recoil. A similar effect was observed for superhydrophobic surfaces with a hierarchal (albeit hydrophobic) structure.[66]

The mechanized abrasion test was conducted with a Taber reciprocating abraser (model 5900) using a CS-8 wearaser abradant as previously described.[54] The superhydrophobicity, including both the CA and SA, exhibited no obvious change after 50 abrasion cycles under a pressure of ~8k Pa. This test demonstrates that the prepared TiO$_2$ nanocomposites have good abrasion resistance.

3.4. Self-Cleaning Properties.
The superhydrophobic properties of the present TiO$_2$–HDPE nanocomposite surface are comparable to traditional superhydrophobic surfaces, even though the nanoparticles are somewhat hydrophilic. The TiO$_2$ particles could, however, provide a new route to a self-cleaning surface as organic molecules as well as microorganisms could be photo-oxidized under UV light.[39,40] Self-cleaning tests were carried out with two types of probe contaminant particles: fine carbon graphite flakes (1 μm average, from Asbury Graphite mills INC. Grade 4827) and course alumina powder (50–130 μm). The TiO$_2$–HDPE nanocomposite surface was coated with the fine particles and mounted on a motorized stage at a fixed angle (13°). The sample was translated at a speed of 1 mm·sec^{-1} beneath the output of a syringe pump (8 μL/s) and particle removal was recorded with a video camera. The impinging velocity of the water droplets mainly depended on the height between the syringe tip and the surface. At a relatively high distance, the water droplets of 8 μL would bounce off the surface so that only the impinging point on the surface was cleaned (as shown in Video SI2 in the Supporting Information). Reducing the height to 5 mm caused the water droplets to roll off the surface as the height was insufficient to induce droplets to bounce. As shown in Video SI3 in the Supporting Information, the water droplets could clean away the course alumina sand as they rolled off the surface.

Removal of fine graphite powder on the superhydrophobic surface is documented in still images (Figure 6a–c). For both
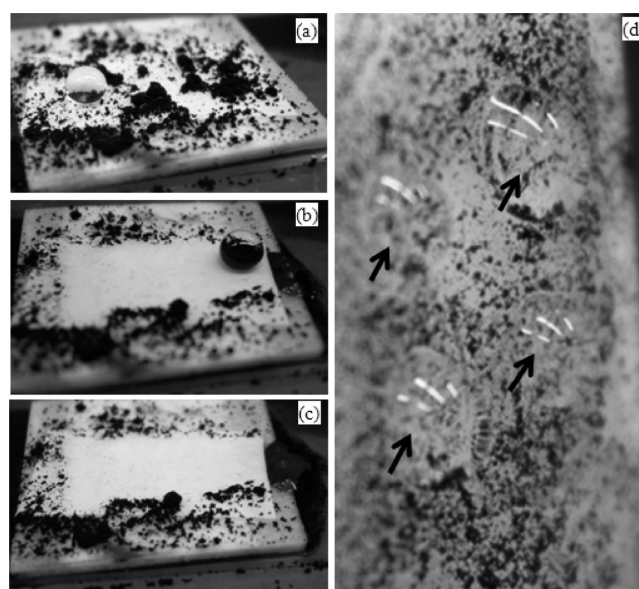

Figure 6. (a–c) Self-cleaning effect of water droplets on the TiO$_2$–HDPE composite superhydrophobic surface, and (d) sticky water droplets (marked) on a normal flat HDPE surface put vertically. The black contaminates are fine carbon particulates with an average size of 1 μm.

types of particles, excellent self-cleaning properties were observed. The particles are wet by the water and imbibed into the droplet as it rolls off the surface. No adverse effects from the hydrophilic TiO$_2$ nanoparticles are apparent. Superhydrophobicity is essential for such self-cleaning particles. When a smooth HDPE surface was used (as received), water droplets adhered to the surface and could neither imbibe the

particles nor roll off the surface, even when the surface was placed at a 90° angle, as shown in Figure 6d. Thus, no self-cleaning properties were observed on a smooth hydrophobic HDPE surface whereas the introduction of roughness enabled self-cleaning to occur, even when a hydrophilic particle accounts, in part, for that roughness.

3.5. UV-Induced Reversible Wettability. The TiO$_2$ nanoparticles used to fabricate these nanocomposites are exposed on the surface of the nanocomposite and have untreated surfaces (i.e., no silanes or surfactants). As a result, the particles are able to interact directly with UV light. UV light has been shown[16] to significantly increase the wettability of TiO$_2$ surfaces as manifested by a decrease in contact angle. The effect of UV light on these hybrid TiO$_2$−HDPE surfaces, however, has not been explored previously and so the contact angle of a droplet on the surface was measured as a function of UV exposure. Exposure experiments were carried out using a UV spot lamp (33 mW cm^{-2}) with a broad output from 320 to 450 nm. The exposure was conducted at room temperature in two environments: dry and with a layer of water resting on the fabricated surface. The change in CA with UV illumination time was monitored and the results are shown in Figure 7a. It can be seen that the CA decreases with the increase of UV illumination time for both surfaces. When submerged in water during illumination, the CA decreased rapidly, falling to 120° in less than 30 min. For the dry surface, the CA decreased slowly at first, dropping only a few degrees during the first 30 min of illumination. Approximately 90 min was required to reach the ultimate contact angle of 120°, more than 3.5 times longer than when the sample was submerged. Under water, no similar induction period was observed. After illuminating for 30 min under water, the TiO$_2$−HDPE surface was heated in a dark oven at 105° for 1.5 h to dry the surface. Superhydrophobicity was restored by this heating process as shown in Figure 7b. This process could be continuously repeated demonstrating good reversible wettability; four cycles are shown in Figure 7b.

It can be seen from Figure 7a that the lowest contact angle for a water droplet on the fabricated surface was measured to be ∼120°; additional UV illumination would not further decrease the CA below 120°. In contrast, surfaces composed of uniformly distributed TiO$_2$ particles exhibit superhydrophilic properties upon UV exposure[17−21] with a CA <10°, whereas HDPE exhibits a CA of 105°, which is independent of UV exposure. On the hybrid surfaces reported here, there are multiple roughness scales and the hydrophilic TiO$_2$ particles are not distributed uniformly, but localized on the posts. As a result, a droplet could transition from a Cassie state to a Wenzel state[68] and fully wet the TiO$_2$-coated posts as shown in Figure 7d. Such a change on the top of the posts triggers the wetting of the HDPE grooves as well. The TCL of a water droplet would be pinned at the edge of the posts. As a result, the contact angle decreased to 120° upon the UV induced wetting of TiO$_2$ This CA is similar to the value reported in our previous study,[51] where we found that the contact angle of a template-embossed pure polyethylene surface (no particles) was 125° in agreement with predictions from the Wenzel equation.

To further increase the extent of wettability change upon UV exposure, we increased the areal fraction of the surface coated with TiO$_2$ nanoparticles by depositing additional particles onto the grooved surface. The nanocomposite surface was immersed into a methanol dispersion containing 0.25% by weight TiO$_2$ nanoparticles for 1 min and then withdrawn at a speed of 0.01
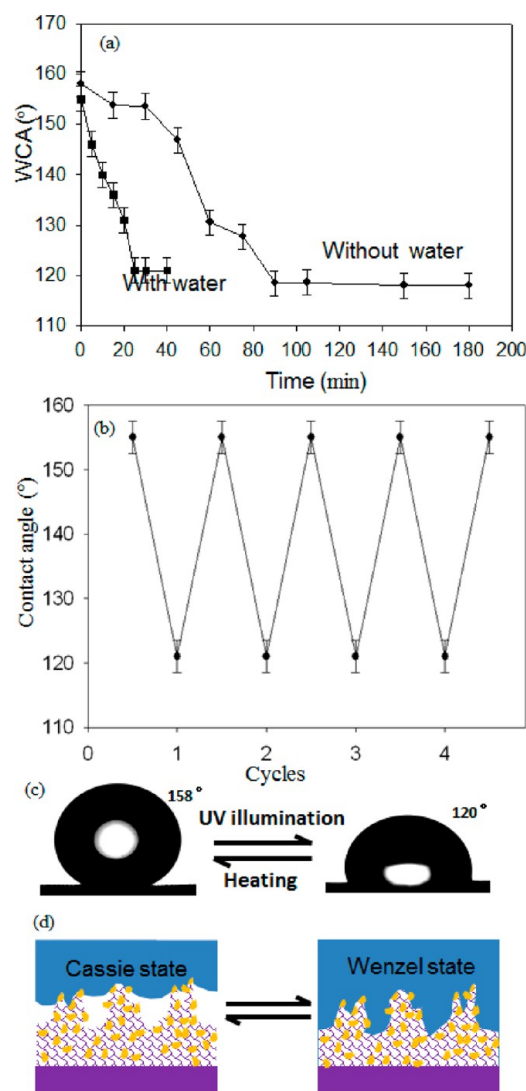

Figure 7. (a) Changes of CA with the UV illumination time with and without water on the surface. (b, c) Reversible wettability changes during cyclic alternation of UV Illumination for 30 min with water, and heating at 105 °C for 1.5 h. (d) Reversible wetting−nonwetting transmission on the fabricated TiO$_2$−polymer nanocomposite surface with hierarchical structures.

mm/s and dried in air at room temperature for 2 min. The dipping process was repeated 5 times to build up a sufficient quantity of particles. The original static CA decreased slightly from 158 to 156° (Figure 4b and Figure SF4a in Supporting Information), whereas the CA after UV illumination decreased significantly from 120° down to 75° as shown in Figure SF4 in the Supporting Information. It is expected that the final CA could be reduced further if a thicker and more uniform TiO$_2$ nanoparticle dispersion could be deposited.

The mechanism responsible for photothermal wetting reversibility was probed by both varying the composition of the nanoparticles embedded into the polymer surface as well as by analyzing the surface with X-ray photoelectron spectroscopy (XPS). A SiO$_2$−HDPE superhydrophobic surface was fabricated using hydrophobic SiO$_2$ nanoparticles in place of the TiO$_2$ particles. This surface is superhydrophobic after fabrication; a droplet maintained on the surface in a sealed environment for more than 24 h remains superhydrophobic with high mobility. Also, the surface remains superhydrophobic
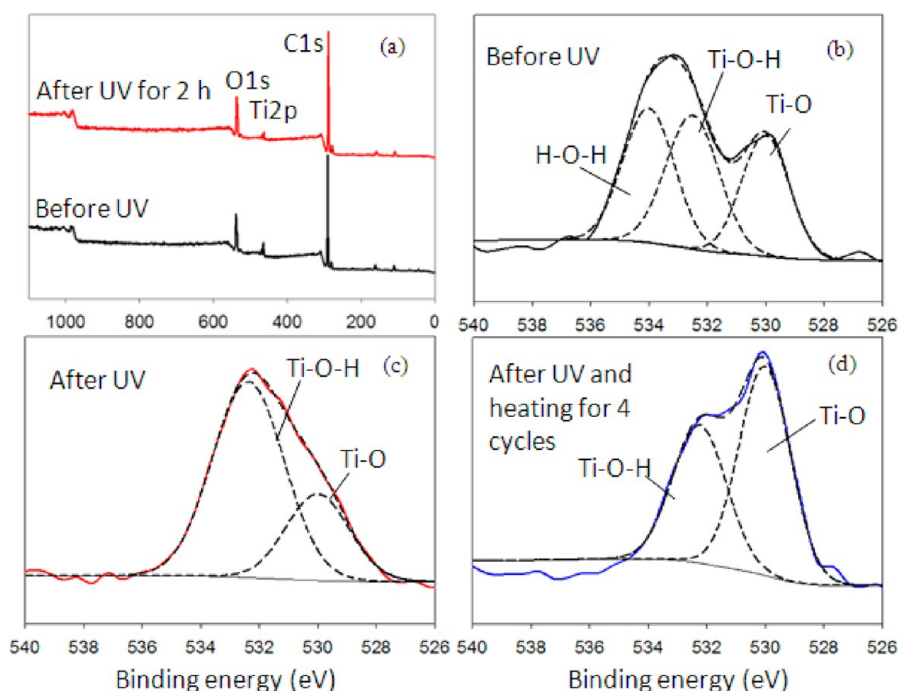
Figure 8. (a) XPS wide-scan survey spectrum of the surfaces before and after UV illumination for 2 h; (b, c) high resolution scan of the O1s peak on different surfaces: (b) as-prepared surface, (c) surface after UV illumination for 2 h without water immersion, (d) surface after 4 cycles of UV illumination and heating.

after illumination by UV light for an hour with water on the surface (same UV power density as used for the TiO_2 experiments). The CA remained at 165° with no change in CA observed.. This comparative experiment indicates that the UV light does not significantly affect the HDPE; it is the photosensitive TiO_2 nanoparticles that accounts for the CA decrease.

The chemical changes on the TiO_2 nanocomposite surface were examined by XPS and the results are shown in Figure 8. The elements C, Ti, and O are clearly visible in the XPS broad spectrum both before and after UV illumination as shown in Figure 8a. The high-resolution spectra of the detected O1s peak on three different surfaces are shown in Figure 8b, c. Before UV illumination (Figure 8b), the O1s of the as-prepared surface was composed of Ti−O (530 eV), Ti−O−H (532.5 eV) and H−O−H (534 eV) bonding, and the atomic ratio of Ti:O was 1:4.4. This indicates that the TiO_2 particles on the as-prepared surface had absorbed a significant amount of water molecules. After UV irradiation of the surface (without water) for 2 h, the O1s was mainly composed of Ti−O and Ti−O−H, and the atomic ratio of Ti:O decreased to 1:6.1. It has been shown[69] that when a TiO_2 surface is irradiated with UV light (λ < 390 nm), an electron−hole pair is generated in the valence and conduction bands of TiO_2, which could react with absorbed H_2O and O_2 molecules on the TiO_2 surface. This would form peroxide intermediates that could further react with the TiO_2 surface to form Ti−O−H bonds. This mechanism is consistent with the observed significant decrease in H−O−H peak (534 eV) and concomitant increase in Ti−O−H bonding at 532.5 eV. Consistent with this observation is the decrease in the Ti:O atomic ratio. The Ti−O−H groups would significantly enhance the hydrophilicity of the TiO_2 nanoparticle surface and so account for the elimination of the free-energy barrier separating the Wenzel and Cassie state[70,71] and the decrease in the CA of a water droplet on the surface. Heating the surface causes the

concentration of Ti−O−H bonds on the surface to decrease. For the surface after 4 cycles of UV illumination and heating, the O1s high-resolution spectra (Figure 8d) was composed of Ti−O and Ti−O−H bonding, but the ratio of Ti−O−H to Ti−O bonding decreased and the Ti:O atomic ratio increased to 1:2 from 1:6.1 after UV irradiation. This indicates that heating at 105 °C for 1.5 h effectively dehydrates the TiO_2 surface and accounts for the restoration of superhydrophobic properties.

Certain studies of superhydrophobic surfaces fabricated with boron nitride nanotubes have shown that the presence of a thin hydrocarbon coating may be responsible for the super-hydrophobic properties on this high energy surface.[72] To exclude the possibility that low-molecular-weight hydrocarbons may be responsible for the superhydrophobicity of the TiO_2−HDPE system reported here, the XPS data were examined to determine the C:Ti ratio before and after baking at 105 °C. The as-prepared surface exhibits a C:Ti ratio of 1:0.17, indicating that the surface is primarily carbon (i.e., HDPE). After UV exposure, the hydrophilic surface has a C:Ti ratio of 1:0.09, consistent with the hydrolysis of Ti and so a small decrease in exposed Ti. After baking, the C:Ti ratio increases to 1:0.32, indicating increased visibility of Ti on the surface. These XPS results indicate that the TiO_2 surface is not covered with a hydrocarbon coating as a result of heating at 105 °C.

To reduce the potential for hydrocarbons diffusing from the HDPE substrate, the use of a lower dehydration temperature was studied. Diffusion of low-molecular-weight species may be possible at temperatures near the melting point of the HDPE crystals. Because the dehydration temperature originally used (105 °C) is near the onset of melting (melt temp peak observed at 133 °C), the diffusion rate could be sufficient should a reservoir of low molecular species be present. Lowering the temperature would significantly reduce diffusion. To test this hypothesis, the dehydration temperature was reduced to 50 °C (more than 80° below T_m). Super-

8922

dx.doi.org/10.1021/am401668y | ACS Appl. Mater. Interfaces 2013, 5, 8915−8924

hydrophobicity was restored after 3 h even at this lower temperature. The XPS measurements and dehydration temperature experiments provide strong evidence that superhydrophobicity is restored by dehydration of the TiO_2 surface.

4. CONCLUSIONS

In summary, a multifunctional TiO_2–HDPE nanocomposite surface, where TiO_2 nanoparticles were segregated into a regular square array pattern, was fabricated by a simple template lamination method. At least three levels of hierarchical roughness were achieved that contribute to the superhydrophobicity, thereby overcoming the relative hydrophilicity of the TiO_2 surface. These roughness levels include: a primary roughness (69 μm pitch) of post and groove features made from embossing a wire mesh template, a secondary roughness (<1 μm pitch) of filaments that result from the infiltration and adhesion of the molten polymer into TiO_2 particles and a tertiary roughness (~20 nm) of TiO_2 particles formed into agglomerates during their manufacture. The as-prepared surfaces exhibited superhydrophobicity immediately after lamination; no surface modification was required. The static CA reaches 158° and the slip-off angle is as low as 8°. When the surface was kept dry and away from UV light, robust superhydrophobic properties were demonstrated. Water droplets released from a height of 30 mm could easily bounce up and roll off a surface tilted at 4°. The surface is also self-cleaning. Water droplets were able to roll off the surface, imbibing and carrying away 1 μm graphite flakes as well as course (50−130 μm) alumina particles at a tilt angle of 13°. Additionally, the TiO_2–HDPE nanocomposite surface shows a UV-thermal induced reversible wettability which can be repeated over numerous cycles. As shown by XPS analysis, the reversible wetting properties are due to hydrolysis of the TiO_2 nanoparticle surface upon irradiation with UV light. This process is accelerated when the surface is immersed in water during illumination. These UV formed Ti−O−H bonds could be reversed by heating, causing the surface composition to revert to primarily Ti−O bonds, which are more hydrophobic. This results in the restoration of superhydrophobic properties. Coating the grooves with a thin, disperse layer of additional TiO_2 particles increases the wettability of the surface upon UV exposure, reducing the minimum contact angle to 75° without significantly affecting the CA in the dehydrated state. The lamination templating fabrication technique with commercially available polymer substrates and nanoparticles is compatible with large-scale lamination processes and so may provide a path to commercially viable products. By anchoring the TiO_2 particles onto the outer surface of the nanocomposite, while ensuring that the TiO_2 particle surface is exposed and not fully embedded within the polymer matrix, efficient use of the nanoparticles is achieved. The combination of superhydrophobicity with photoactivity provides a unique multifunctional surface. By reducing opportunities for microbial adhesion through superhydrophobicity and inactivating microbes with UV light that may attach to the surface, an effective antimicrobial material could be produced. Future work will explore the applicability of this type of material for antimicrobial surfaces, water purification, and the photocatalytic degradation of organic compounds.

■ ASSOCIATED CONTENT

ⓢ Supporting Information

Differential scanning calorimeter results for HDPE, low magnification of EDX images of the fabricated surface, and three videos. This material is available free of charge via the Internet at http://pubs.acs.org.

■ AUTHOR INFORMATION

Corresponding Author

*E-mail: alan.lyons@csi.cuny.edu.

Notes

The authors declare no competing financial interest.

■ ACKNOWLEDGMENTS

■ REFERENCES

(1) Lafuma, A.; Quere, D. *Nat. Mater.* **2003**, *2*, 457−460.
(2) Li, X. M.; Reinhoudt, D.; Crego-Calama, M. *Chem. Soc. Rev.* **2007**, *36*, 1350−1368.
(3) Quere, D. *Annu. Rev. Mater. Res.* **2008**, *38*, 71−99.
(4) Crick, C. R.; Parkin, I. P. *Chem.—Eur. J.* **2010**, *16*, 3568−3588.
(5) Liu, K.; Jiang, L. *ACS Nano* **2011**, *5*, 6786−6790.
(6) Yao, X.; Song, Y.; Jiang, L. *Adv. Mater.* **2011**, *23*, 719−734.
(7) Mumm, F.; van Helvoort, A. T. J.; Sikorski, P. *ACS Nano* **2009**, *3*, 2647−2652.
(8) Park, Y. B.; Im, M.; Im, H.; Choi, Y. K. *Langmuir* **2010**, *26*, 7661−7664.
(9) Lapierre, F.; Thomy, V.; Coffinier, Y.; Blossey, R.; Boukherroub, R. *Langmuir* **2009**, *25*, 6551−6558.
(10) Cao, L.; Jones, A. K.; Sikka, V. K.; Wu, J.; Gao, D. *Langmuir* **2009**, *25*, 12444−12448.
(11) Bravo, J.; Zhai, L.; Wu, Z.; Cohen, R. E.; Rubner, M. F. *Langmuir* **2007**, *23*, 7293−7298.
(12) Xu, Q. F.; Wang, J. N.; Sanderson, K. D. *ACS Nano* **2010**, *4*, 2201−2209.
(13) Zhang, X.; Shi, F.; Niu, J.; Jiang, Y.; Wang, Z. *J. Mater. Chem.* **2008**, *18*, 621−633.
(14) Watanabe, T. *J. Ceram. Soc. Jpn.* **2009**, *117*, 1285−1292.
(15) Yamashita, H.; Nakao, H.; Takeuchi, M.; Nakatani, Y.; Anpo, M. *Nucl. Instrum. Methods Phys. Res., Sect. B* **2003**, *206*, 898−901.
(16) Wang, S.; Songa, Y.; Jiang, L. *J. Photochem. Photobiol. C* **2007**, *8*, 18−29.
(17) Feng, X.; Zhai, J.; Jiang, L. *Angew. Chem., Int. Ed.* **2005**, *44*, 5115−5118.
(18) Zhang, X.; Jin, M.; Liu, Z.; Nishimoto, S.; Saito, H.; Murakami, T.; Fujishima, A. *Langmuir* **2006**, *22*, 9477−9479.
(19) Zhang, X.; Jin, M.; Liu, Z.; Tryk, D. A.; Nishimoto, S.; Murakami, T.; Fujishima, A. *J. Phys. Chem. C* **2007**, *111*, 14521−14529.
(20) Zhang, X.; Kono, H.; Liu, Z.; Nishimoto, S.; Tryk, D. A.; Murakami, T.; Sakai, H.; Abeb, M.; Fujishima, A. *Chem. Commun.* **2007**, *46*, 4949−4951.
(21) Lai, Y.; Huang, J.; Gong, J.; Huang, Y.; Wang, C.; Chen, Z.; Lin, C. *J. Electrochem. Soc.* **2009**, *156*, 480−484.
(22) Zhang, F.; Chen, S.; Dongb, L.; Lei, Y.; Liu, T.; Yin, Y. *Appl. Surf. Sci.* **2011**, *257*, 2587−2591.
(23) Jin, R. H.; Yuan, J. J. *Adv. Mater.* **2009**, *21*, 3750−3753.
(24) Wang, D.; Wang, X.; Liu, X.; Zhou, F. *J. Phys. Chem. C* **2010**, *114*, 9938−9944.

(25) Nishimoto, S.; Sekine, H.; Zhang, X.; Liu, Z.; Nakata, K.; Murakami, T.; Koide, Y.; Fujishima, A. *Langmuir* **2009**, *25*, 7226−7228.

(26) Lim, H. S.; Kwak, D.; Lee, D. Y.; Lee, S. G.; Cho, K. *J. Am. Chem. Soc.* **2007**, *129*, 4128−4129.

(27) Liu, H.; Feng, L.; Zhai, J.; Jiang, L.; Zhu, D. B. *Langmuir* **2004**, *20*, 5659−5661.

(28) Feng, X.; Feng, L.; Jin, M.; Zhai, J.; Jiang, L.; Zhu, D. *J. Am. Chem. Soc.* **2004**, *126*, 62−63.

(29) Li, G. P; Chen, T.; Yan, B.; Ma, Y.; Zhang, Z.; Yu, T.; Shen, Z.; Chen, H.; Wu, T. *Appl. Phys. Lett.* **2008**, *92*, 173104.

(30) Liu, Y.; Lin, Z.; Lin, W.; Moon, K. S.; Wong, C. P. *ACS Appl. Mater. Interfaces* **2012**, *4*, 3959−3964.

(31) Sakai, M.; Kono, H.; Nakajima, A.; Zhang, X.; Sakai, H.; Abe, M.; Fujishima, A. *Langmuir* **2009**, *25*, 14182−14186.

(32) Kwak, G.; Seol, M.; Tak, Y.; Yon, K. *J. Phys. Chem. C* **2009**, *113*, 12085−12089.

(33) Papadopoulou, E. L.; Barberoglou, M.; Zorba, V.; Manousaki, A.; Pagkozidis, A.; Stratakis, E.; Fotakis, C. *J. Phys. Chem. C* **2009**, *113*, 2891−2895.

(34) Zhang, Q.; Wang, J. *Int. J. Chem. React. Eng.* **2010**, *8*, 1−10.

(35) Kamegawa, T.; Shimizu, Y.; Yamashita, H. *Adv. Mater.* **2012**, *24*, 3697−3700.

(36) Crick, C. R.; Bear, J. C.; Kafizas, A.; Parkin, I. P. *Adv. Mater.* **2012**, *24*, 3505−3508.

(37) Wang, R.; Hashimoto, K.; Fujishima, A.; Chikuni, M.; Kojima, E.; Kitamura, A.; Shimohigoshi, M.; Watanabe, T. *Nature* **1997**, *388*, 431−432.

(38) Fujishima, A.; Honda, K. *Nature* **1972**, *238*, 37−38.

(39) Chung, C.; Lin, H.; Tsou, H.; Shi, Z.; He, J. *J. Biomed. Mater. Res. B* **2008**, *85*, 220−224.

(40) Chorianopoulos, N. G.; Tsoukleris, D. S.; Panagou, E. Z.; Falaras, P.; Nychas, G. J. E. *Food Microbiol.* **2011**, *28*, 164−170.

(41) Rico, V.; Lopez, C.; Borras, A.; Espinos, J. P.; Gonzalez−Elipe, A. R. *Sol. Energy Mater. Sol. Cells* **2006**, *90*, 2944−2949.

(42) Hsieh, C. T.; Lai, M. H.; Cheng, Y. S. *J. Colloid Interface Sci.* **2009**, *340*, 237−242.

(43) Zhu, J.; Xiea, J.; Lu, X.; Jiang, D. *Colloids Surf. A* **2009**, *342*, 97−101.

(44) Lai, Y.; Lin, C.; Huang, J.; Zhuang, H.; Sun, L.; Nguyen, T. *Langmuir* **2008**, *24*, 3867−3873.

(45) Caputo, G.; Nobile, C.; Kipp, T.; Blasi, L.; Grillo, V.; Carlino, E.; Manna, L.; Cingolani, R.; Cozzoli, P. D.; Athanassiou, A. *J. Phys. Chem. C* **2008**, *112*, 701−714.

(46) Lai, Y.; Gao, X.; Zhuang, H.; Huang, J.; Lin, C.; Jiang, L. *Adv. Mater.* **2009**, *21*, 3799−3803.

(47) Nakata, K.; Nishimoto, S.; Yuda, Y.; Ochiai, T.; Murakami, T.; Fujishima, A. *Langmuir* **2010**, *26*, 11628−11630.

(48) Hozumi, A.; Cheng, D. F.; Yagihashi, M. *J. Colloid Interface Sci.* **2011**, *353*, 582−587.

(49) Xu, X.; Zhang, Z. Z.; Liu, W. *Colloid Surf. A* **2009**, *341*, 21−26.

(50) Lai, Y.; Pan, F.; Xu, C.; Fuchs, H.; Chi, L. *Adv. Mater.* **2013**, *25*, 1682−1686.

(51) Zhao, X.; Zhao, Q.; Yu, J.; Liu, B. *J. Non-Cryst. Solids* **2008**, *354*, 1424−1430.

(52) Sun, W.; Zhou, S.; Chen, P.; Peng, L. *Chem. Commun.* **2008**, *5*, 603−605.

(53) Allouni, Z. E.; Hol, P. J.; Cauqui, M. A.; Gjerdet, N. R.; Cimpan, M. R. *Toxicol. Vitro* **2012**, *26*, 469−479.

(54) Xu, Q. F.; Mondal, B.; Lyons, A. M. *ACS Appl. Mater. Interfaces* **2011**, *3*, 3508−3514.

(55) Barthlott, W.; Neinhuis, C. *Planta* **1997**, *202*, 1−8.

(56) Gao, L. C.; McCarthy, T. J. *Langmuir* **2006**, *22*, 2966−1967.

(57) Lee, C. H.; Jung, P. G.; Lee, S. M.; Park, S. H.; Shin, B. S.; Kim, J.; Hwang, K.; Kim, K. M.; Ko, J. S. *J. Micromech. Microeng.* **2010**, *20*, 035018.

(58) Furmidge, C. G. L. *J. Colloid Sci.* **1962**, *17*, 309−324.

(59) Extrand, C. W.; Gent, A. N. *J. Colloid Interface Sci.* **1990**, *138*, 431−442.

(60) Cassie, A. B. D.; Baxter, S. *Trans. Faraday Soc.* **1944**, *40*, 546−551.

(61) Marmur, A. *Langmuir* **2003**, *19*, 8343−8348.

(62) Marmur, A. *Langmuir* **2008**, *24*, 7573−7579.

(63) Barthlott, W.; Schimmel, T.; Wiersch, S.; Koch, K.; Brede, M.; Barczewski, M.; Walheim, S.; Weis, A.; Kaltenmaier, A.; Leder, A.; Bohn, H. F. *Adv. Mater.* **2010**, *22*, 2325−2328.

(64) Balani, K.; Batista, R. G.; Lahiri, D.; Agarwal, A. *Nanotechnology* **2009**, *20*, 305707.

(65) Deng, T.; Varanasi, K. K.; Hsu, M.; Bhate, N.; Keimel, C.; Stein, J.; Blohm, M. *Appl. Phys. Lett.* **2009**, *94*, 133109.

(66) Chen, L.; Xiao, Z.; Chan, P. C. H.; Lee, Y.; Li, Z. *Appl. Surf. Sci.* **2011**, *257*, 8857−8863.

(67) Maynes, D.; Johnson, M.; Webb, B. W. *Phys. Fluids* **2011**, *23*, 052104.

(68) Wenzel, R. N. *Ind. Eng. Chem.* **1936**, *28*, 988−994.

(69) Chen, X.; Mao, S. S. *Chem. Rev.* **2007**, *107*, 2891−2959.

(70) Tuteja, A.; Choi, W.; Ma, M.; Mabry, J. M.; Mazzella, S. A.; Rutledge, G. C.; Mckinley, G. H.; Cohen, R. E. *Science* **2007**, *318*, 1618−1622.

(71) Koishi, T.; Yasuoka, K.; Fujikawa, S.; Ebisuzaki, T.; Zeng, X. C. *Proc. Natl. Acad. Sci. U.S.A.* **2009**, *106*, 8435−8440.

(72) Boinovich, L. B.; Emelyanenko, A. M.; Pashinin, A. S.; Lee, C. H.; Drelich, J.; Yap, Y. K. *Langmuir* **2012**, *28*, 1206−1216.